UDCT: Unsupervised data to content transformation with histogram-matching cycle-consistent generative adversarial networks

Stephan Johannes Ihle[1], Andreas M. Reichmuth[1], Sophie Girardin[1], Hana Han[1], Flurin Stauffer[1], Anne Bonnin[2], Marco Stampanoni[2], Karthik Pattisapu[1], János Vörös[1*], Csaba Forró[1*]

June 5, 2019

[1]Laboratory of Biosensors and Bioelectronics, ETH Zurich, Gloriastrasse 35, 8092 Zurich, Switzerland
[2]Paul Scherrer Inst, Swiss Light Source, CH-5232 Villigen, Switzerland

Supplementary Information

The supplementary videos S1 to S4 can be found at https://downloads.lbb.ethz.ch/Videos/

Network formulation

Let $A \in [0,1]^{n\times m\times a}$ be the set of real images with dimensions n by m and a channels. Furthermore, $B \in [0,1]^{n\times m\times b}$ be the set of synthetic images of same size and b channels. The generators $\mathcal{G}_B : A \to B$ and $\mathcal{G}_A : B \to A$ transform a real image into a synthetic images and a synthetic image to a real one, respectively. The discriminator $\mathcal{D}_\mathcal{X} : \mathcal{X} \to [0,1]$ where $\mathcal{X} \in \{A, B\}$ predicts, whether a data sample is either a genuine image (real or synthetic) or a generated image. A genuine image was encoded with a 0, while a generated image is encoded with a 1. The histogram discriminator $\mathcal{H}_\mathcal{X} : \mathbb{R}^h \to [0,1]$ functions as $\mathcal{D}_\mathcal{X}$ with the exception that it will get a binned inverse cumulative distribution function ($\mathrm{iCDF}_h(\cdot)$) of the input image with h bins.

In the following, the network architecture is described. Let `cUsV-W` be a `U` × `U` convolution layer with stride `V` and `W` filters. Futhermore, `IN` denotes an InstanceNorm layer, `ReLU` a rectified linear unit activation, `leaky_ReLU` a leaky rectified linear unit activation with (alpha = 0.2), and `tanh` a hyperbolic tangent activation function. The shorthand for a fractional-strided `U` × `U` convolution layer with stride `1/V` and `W` filters is `ctUsV-W`. A residual addition is signified with `r<`. The layer to which the network is added is marked with the most recent `>` before the residual layer. A fully connected layer with `W` nodes and a dropout probability of 50% is defined as `dW`. Finally, `pU` describes a 2 dimensional reflective padding step.

Generator The generators are built in a similar fashion as the generator with 6 residual layers proposed by Zhu et al. [1]. Below, $\mathcal{W}$ describes the number of channels in the output domain (a or b).

`p3 c7s1-64, IN, ReLU`
`p1, c3s2-128, IN, ReLU`
`p1, c3s2-256, IN, ReLU`
`>, p1, c3s1-256, IN, ReLU, p1, c3s1-256, IN, r<` [repeat 6 times]
`ct3s2-128, IN, ReLU`
`ct3s2-64, IN, ReLU`
`c7s3-`$\mathcal{W}$`, IN, tanh/2 + 0.5`

Discriminator Both discriminators are identical to the discriminator introduced in Zhu et al. [1]. The discriminator has a receptive field of size 70 × 70.

`p1, c4s2-64, leaky_ReLU`
`p1, c4s2-128, IN, leaky_ReLU`

```
p1, c4s2-256, IN, leaky_ReLU
p1, c4s1-512, IN, leaky_ReLU
p1, c4s1-1
```

Histogram discriminator The histogram discriminator gets an inverse cumulative distribution function (iCDF) as input. The iCDF can be transformed into a histogram. However, it is easier to create, since it is equivalent to the intensity-sorted pixel values of an image. To reduce the complexity of the network, the iCDF is binned into h by taking the mean of all the elements belonging to the bin. Since h was set to n, the number of averaged values for each bin was m. If an image had multiple channels, each channel was binned separately from each other. Afterwards, the channel histograms were concatenated and fed into the network.

The histogram discriminator is a multi-layer perceptron with two hidden layers.

```
d64, tanh, d64, tanh, d1 + 0.5
```

Losses

The total loss of the network can be described by:

$$\mathcal{L}_{\text{total}} = \mathcal{L}_{\text{dis\_A}} + \mathcal{L}_{\text{dis\_B}} + \lambda_c \cdot \mathcal{L}_{\text{cyc}}, \tag{S1}$$

where λ_c is an arbitrary value weighting the cycle-consistent loss against the adversarial losses. The terms on the right side are defined below. The optimizer is trying to solve:

$$\mathcal{G}_A^*, \mathcal{G}_B^*, \mathcal{D}_A^*, \mathcal{D}_B^*, \mathcal{H}_A^*, \mathcal{H}_B^* = \underset{\mathcal{G}_A^*, \mathcal{G}_B^*}{\operatorname{argmin}} \underset{\mathcal{D}_A^*, \mathcal{D}_B^*}{\operatorname{argmax}} \underset{\mathcal{H}_A^*, \mathcal{H}_B^*}{\operatorname{argmax}} \mathcal{L}_{\text{total}} \tag{S2}$$

The network is implemented with two optimizers. The first one trains the four discriminators by maximizing equation (S2), while the second one trains the two generators by minimizing equation (S2).

Adversarial loss The adversarial loss used in this work is the same as the usual least-square loss for GANs with the addition of the loss function given by the histogram discriminator. The optimizer for the discriminators tries to maximize the adversarial losses. In the equation below, $\mathcal{X}$ is either A or B.

$$\begin{aligned}\mathcal{L}_{\text{dis\_}\mathcal{X}} = &\mathbb{E}_{x \sim p_{\text{data}}}\left[(1 - \mathcal{D}_\mathcal{X}(x))^2\right] + \mathbb{E}_{y \sim p_{\text{data}}}\left[(\mathcal{D}_\mathcal{X}(\mathcal{G}_\mathcal{X}(y)))^2\right] \\ &+ \lambda_h \cdot \left(\mathbb{E}_{x \sim p_{\text{data}}}\left[(1 - \mathcal{H}_\mathcal{X}(x))^2\right] + \mathbb{E}_{y \sim p_{\text{data}}}\left[(\mathcal{H}_\mathcal{X}(\mathcal{G}_\mathcal{X}(y)))^2\right]\right)\end{aligned} \tag{S3}$$

Cycle-consistent loss The cycle-consistent loss encourages the generators to approximate a bijective mapping between the relevant subsets of A and B. The cycle-consistent loss consists of a loss term for the cycle $A \to B \to A$ and a term for the cycle $B \to A \to B$.

$$\mathcal{L}_{\text{cyc}} = \mathbb{E}_{x \sim p_{\text{data}}}\left[(x - \mathcal{G}_A(\mathcal{G}_B(x)))^2\right] + \mathbb{E}_{y \sim p_{\text{data}}}\left[(y - \mathcal{G}_B(\mathcal{G}_A(y)))^2\right] \tag{S4}$$

Generator loss The two generator losses are used to train the generators. The generator optimizer is trying to minimize these losses. The cycle-consistent loss is divided by a factor of two in order to make the overall loss identical to the one given in equation (S1).

$$\mathcal{L}_{\text{gen\_}\mathcal{X}} = \mathbb{E}_{y \sim p_{\text{data}}}\left[(\mathcal{D}_\mathcal{X}(\mathcal{G}_\mathcal{X}(y)))^2\right] + \lambda_h \cdot \mathbb{E}_{y \sim p_{\text{data}}}\left[(\mathcal{H}_\mathcal{X}(\mathcal{G}_\mathcal{X}(y)))^2\right] + \frac{\lambda_c}{2} \cdot \mathcal{L}_{\text{cyc}} \tag{S5}$$

Training

Unless otherwise stated, each dataset has been trained with a λ_c of 10 and a λ_h of 0. An optimizer ($\beta_1 = 0.5$, $\beta_2 = 0.999$, $\epsilon = 10^{-8}$) has been used to MinMax equation (S2). Each network has been trained for 200 epochs. The learning rate was fixed to 0.0002 for the first 100 epochs. Afterwards it linearly decayed to 0 for the next 100 epochs. As in Zhu et al. [1], all convolutional kernels were initialized from a Gaussian distribution (mean: 0, std: 0.02). In order to achieve a more consistent cyclic behaviour, noise was added to the input of all discriminators. The noise added was Gaussian noise with standard deviation of 0.9^n where n is the current epoch. In order to follow the implementation of Zhu et al. as close as possible, a buffer was introduced that stored 50 previously generated images on which the discriminator were trained as described by Shrivastava et al. [2]. The batchsize was fixed to 4. The buffer was filled with all 4 images until it was full. Afterwards, four random elements in the buffer were replaced with new ones. Following the suggestion of Shrivastava et al., the discriminators were trained with 2 images from the buffer and 2 current ones. The networks have been trained on a GeForce RTX 2080 Ti (Nvidia Corporation, USA). Training a network for one iteration took about 1 sec. Therefore, training a network on the *C. elegans* for 200 epochs took roughly 10 hours. For the neuronal bright field images, the biggest dataset discussed here, the total training took about a day.

VGG-Cells

With the synthetic dataset displayed on Fig.2b), we localize cells to within 2 pixels on average from their ground truth position. The distribution of distance between a detected cell and its closest ground-truth position is displayed on Fig.S1.

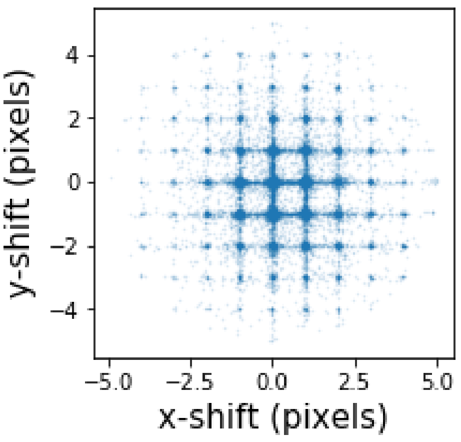

Figure S1: Distance-vectors between detected VGG Cells centers and the ground truth labels in x-y pixel shift units, displaying 34'000 detected cells. Each point displays the x-y shift between a generator cell's position and the nearest ground-truth label. The average error on the location of the cell-center is 1.25 pixels. These numbers are fractional because the maximum likelihood estimation of the centers of the Gaussians in the transformed dataset yield real and not integer numbers.

On average we count 95.4% of the cells. Because we operate in an unsupervised fashion, we do not directly minimize the counting error during training. We notice however that some cells would not be counted either by a human, as shown in Fig.S2. Indeed, the ground-truth labels used to create the VGG Cells dataset in some cases can be so close to one another that the generated cell ensemble they represent only looks like a single cell. If a human cannot distinguish these cells, our cycleGAN approach cannot either. However, the number of cell-centers that are within a few pixels of one another shows as expected a pure N^2 dependency, where N is the number of cells-centers in an image (see Fig.S2). This means that a supervised network can easily minimize its count error by adding a bias of aN^2 to its count N, in order to reduce the counting gap. If we take our raw cycleGAN cell count based on the results of Fig.2b, that we define as c, for each image and let $c + \alpha c^2$ be a modified count and minimize the error against the true counts, we bring down our mean average error to 4 cells per image.

Color-coding neuron location

The color of each neuron in the synthetic images of the color-coded neuron dataset only depends on the center location of each neuron. Let $C_p \in \{0,1\}^{n\times m}$ be one, if the pixel describes the center of a neuron in the p^{th} synthetic image and zero otherwise. Furthermore, let $K \in \mathbb{R}^{101\times101\times3}$ be a kernel used for determining the

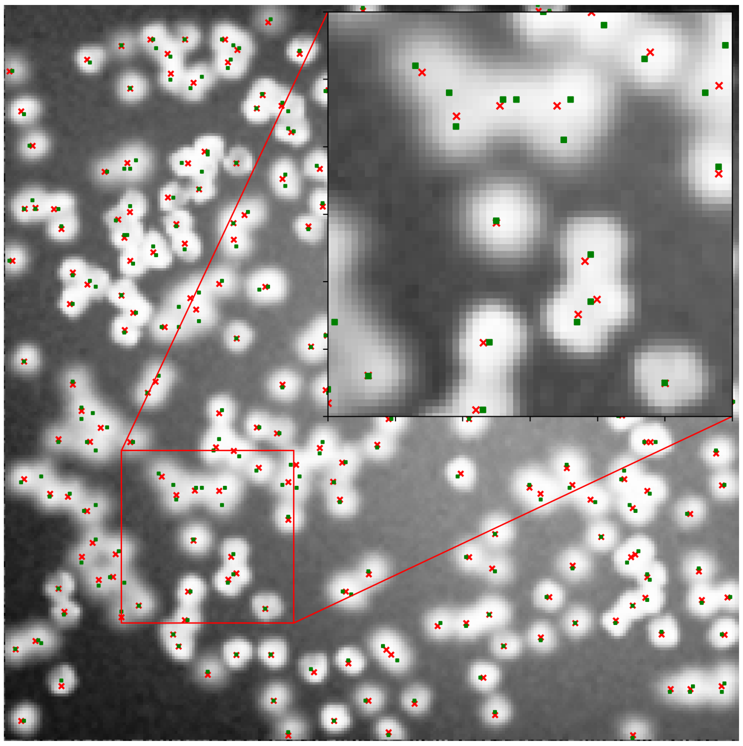

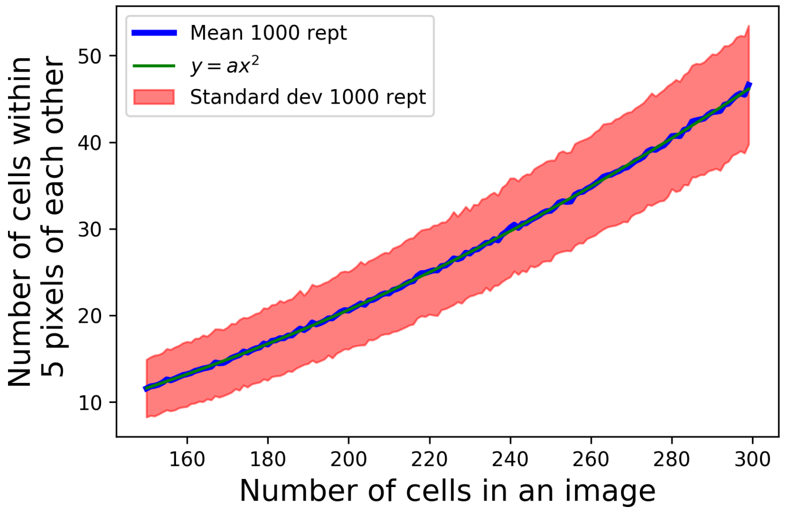

Figure S2: **Issues with VGG cells dataset**: *Top*: the green dots are the ground-truth positions of the cells of the VGG dataset. The red dots are the cell-center locations detected by our cycleGAN method displayed in Fig.2b. The inset shows that in some cases even a human could not count the cells correctly based on the ground-truth positions. This is particularly evident in the top part of the inset. *Bottom*: We distributed N cells-centers randomly in 256×256 pixel space, and counting how many are within m (here 5) pixels of each other and repeated it a 1000 times. The blue curve shows the mean number of such cells, and the red spread is the standard deviation of the 1000 repetitions. The number of such cells follows an N^2 relation. This means that when a supervised network minimizes the error count, although it may inherently count the same cells as our cycleGAN, it has the ability to easily correct for the error by adding a bias of αx^2, where x is what the network would truly count.

colors. The neuron in the p^{th} image with location (u, v) is getting an rgb color vector of

$$\frac{\tanh\left([C_p(\cdot,\cdot) * K(\cdot,\cdot,k)](u,v)\right) + 1}{2}, \tag{S6}$$

where $k \in \{\text{red}, \text{green}, \text{blue}\}$ describes the channel. The kernel K is shown in Figure (S3) and can be fully described by the matrix $\{\mathbf{K}\}_{i,j}$:

$$K = [\mathbf{K}^{\mathrm{T}}; 1 - \mathbf{K}; \mathbf{K}] \tag{S7}$$

with

$$\mathbf{K}_{i,j} = f(i) \cdot g(j), \qquad i, j \in \{1, 2, \ldots, 101\}, \tag{S8}$$

where the functions $f(\cdot)$ and $g(\cdot)$ are defined as

$$f(i) = \begin{cases} \max\left\{ \min\left\{\frac{3.75}{i}, 3\right\}, -3 \right\} & \text{if } i \neq 50 \\ 0 & \text{if } i = 50 \end{cases} \tag{S9}$$

and

$$g(j) = \begin{cases} \min\left\{\frac{3.75}{|j|}, 3\right\} & \text{if } j \neq 50 \\ 3 & \text{if } j = 50. \end{cases} \tag{S10}$$

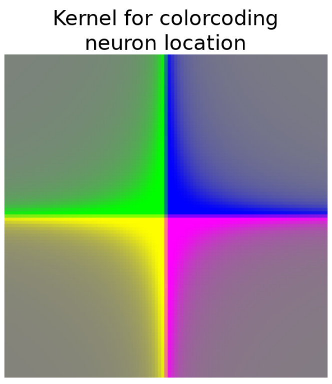

Figure S3: The kernel K used to determine the color of each neuron in the synthetic dataset. The color only depends on the relative location of a neuron with respect to other neurons.

C. elegans dataset

The number of worms put in the synthetic dataset influences the quality of the cycles. In this case, the synthetic dataset does not have enough worms.

Primary cortical neurons dataset : Example of a backchannel

We illustrate here the issue that can arise without histogram loss in Fig.S5. On the top row, Fig.S5a shows the raw image cycle. Because of the residual network in the generator, part of the image is compressed into the generated image, but not clearly visible at all. However it is perfectly retrieved in the cycle. We call this a backchannel, as the original image is somehow retrieved through the cycle, without having a proper generated image.
This backchannel is much more difficult for the network to achieve in the synthetic cycle shown in Fig.S5b. We hypothesize that this is due to the fact that there is only 1 channel available in the generated (raw domain) image.
The effect of the histogram loss is more thoroughly discussed in Fig.S7.

Importance of variation in synthetic images

We display the importance of having enough variation in the synthetic dataset to generate realistic raw images in Fig.S6. CNNs and therefore GANs are deterministic functions: for the same input they always generate the same output. Real objects like neurons on a glass slide come in different kinds of shapes, size, and brightness.

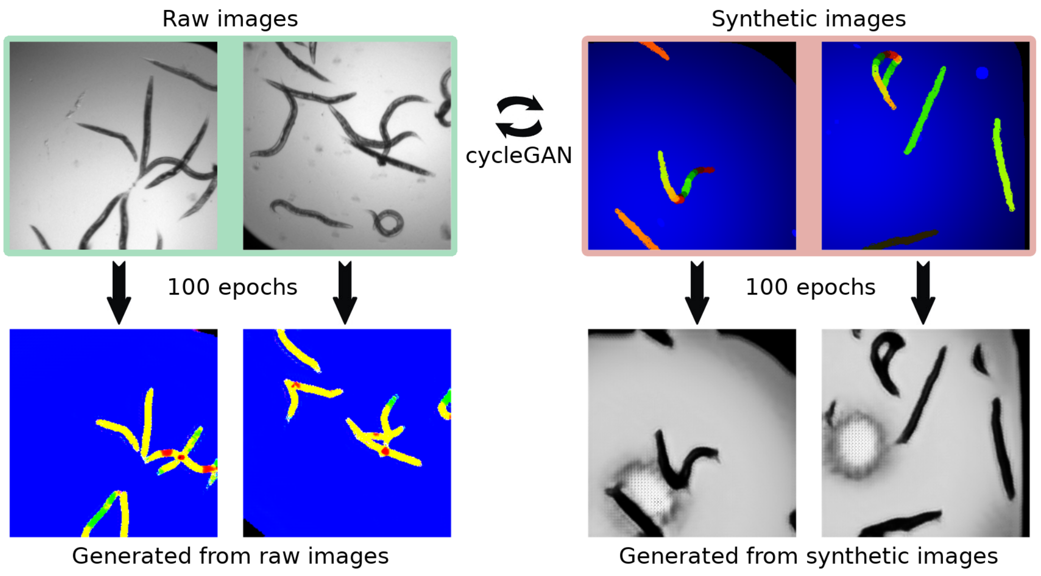

Figure S4: An example synthetic dataset with approximately half the number of worms as in the raw dataset. Especially in raw images with a lot of worms, some worms are removed by the generator (bottom left). The opposite effect occurs in the generator that creates raw images (bottom right), where worms are created out of the background and the image boundary.

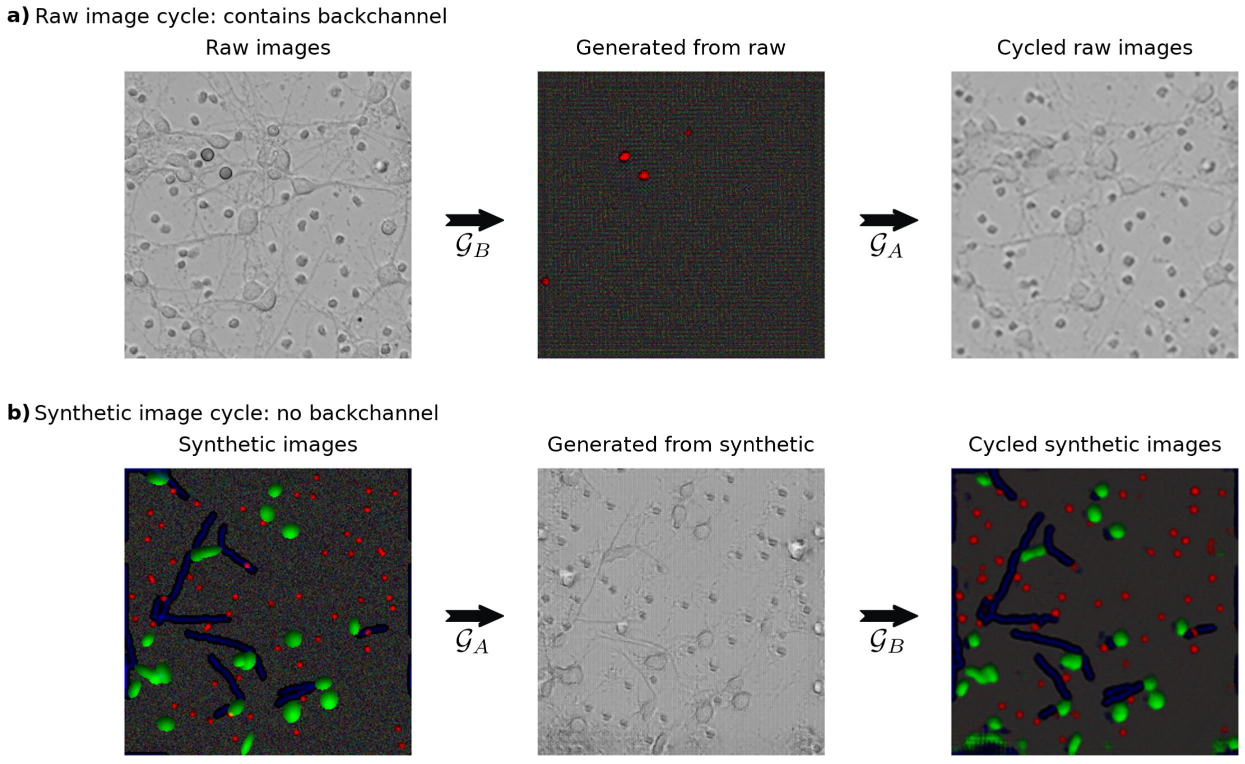

Figure S5: The figure shows backchannel. For the raw image cycle (a), a raw image is mapped to a generated synthetic image without any clear relationship. However, the cycled image is a close match to the original image. At the same time, the synthetic image cycle (b) appears to function as desired.

Therefore, the synthetic ellipses that should represent them in the synthetic data should bear similar amounts of variation. Otherwise, the complexity of real neurons will not be generated as visible on the left side of Fig.S6. On the other hand, by varying slightly the shape, the intensity profile and the background noise, we can create much more realistic pictures. Although we are only interested in the synthetic-looking generated pictures for the analysis, since those are the transformed raw images, it is very important to have a good cycle both in the raw and the synthetic cycle to have a good mapping between synthetic and raw data.

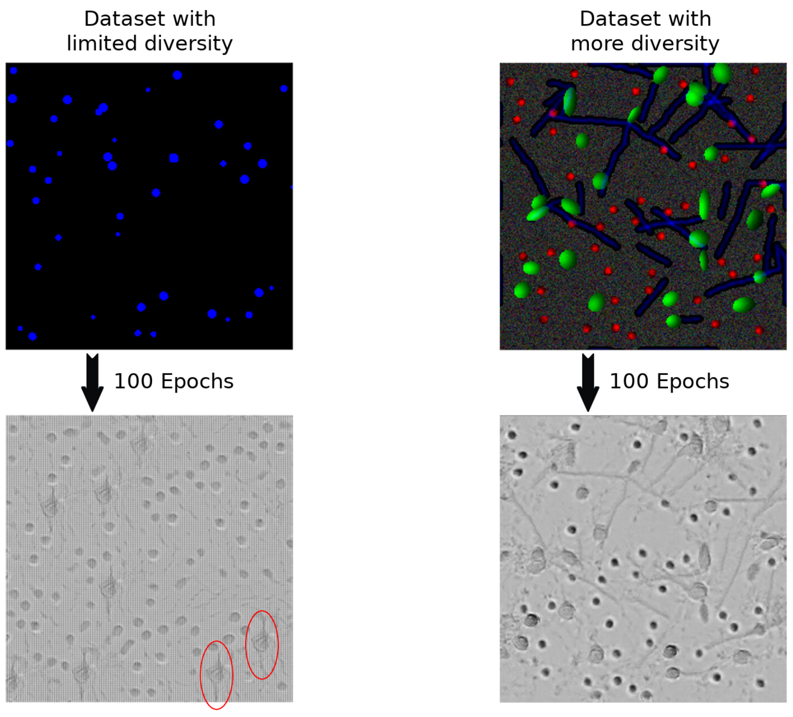

Figure S6: The effect that the diversity of a dataset can have on the generated images. The brightfield neuronal images were trained with a cycleGAN using two different synthetic datasets. When the diversity of the dataset was low (left side), repetitive patterns occur in the generated images (see circled data). When the complexity of the synthetic dataset is higher (right side), the alive neurons can exhibit a wider range of possible shapes. Both networks have been trained for 100 epochs.

Importance of histogram loss

On Fig.S7 we compare the generated images with and without histogram loss. One can see that quite often, the synthetic-looking generated pictures without histogramm loss (second row of green shaded panel on Fig.S7) are often not good. This goes back to the backchannels discussed in Fig.S5.

Mean absolute and relative error

The mean absolute and relative error of the neuronal counts is given in Table (S2) and (2) for the bright-field cortical neurons, respectively. The mean absolute error is defined as

$$\mathrm{Error}_{\mathrm{abs}} = \frac{1}{|\Omega|} \sum_{i\in\Omega} |\mathrm{pred}_i - \mathrm{gt}_i|, \tag{S11}$$

where Ω is the set of all datapoints, $|\Omega|$ the number of elements in Ω, pred_i the number of predicted neurons for the i^{th} datapoint, and gt_i the corresponding groundtruth. In a similar fashion, the mean relative error is defined as

$$\mathrm{Error}_{\mathrm{abs}} = \frac{1}{|\Omega|} \sum_{i\in\Omega} \begin{cases} 1 - \frac{\min\{\mathrm{pred}_i, \mathrm{gt}_i\}}{\max\{\mathrm{pred}_i, \mathrm{gt}_i\}} & \text{if } \max\{\mathrm{pred}_i, \mathrm{gt}_i\} \neq 0 \\ 0 & \text{if } \max\{\mathrm{pred}_i, \mathrm{gt}_i\} = 0. \end{cases} \tag{S12}$$

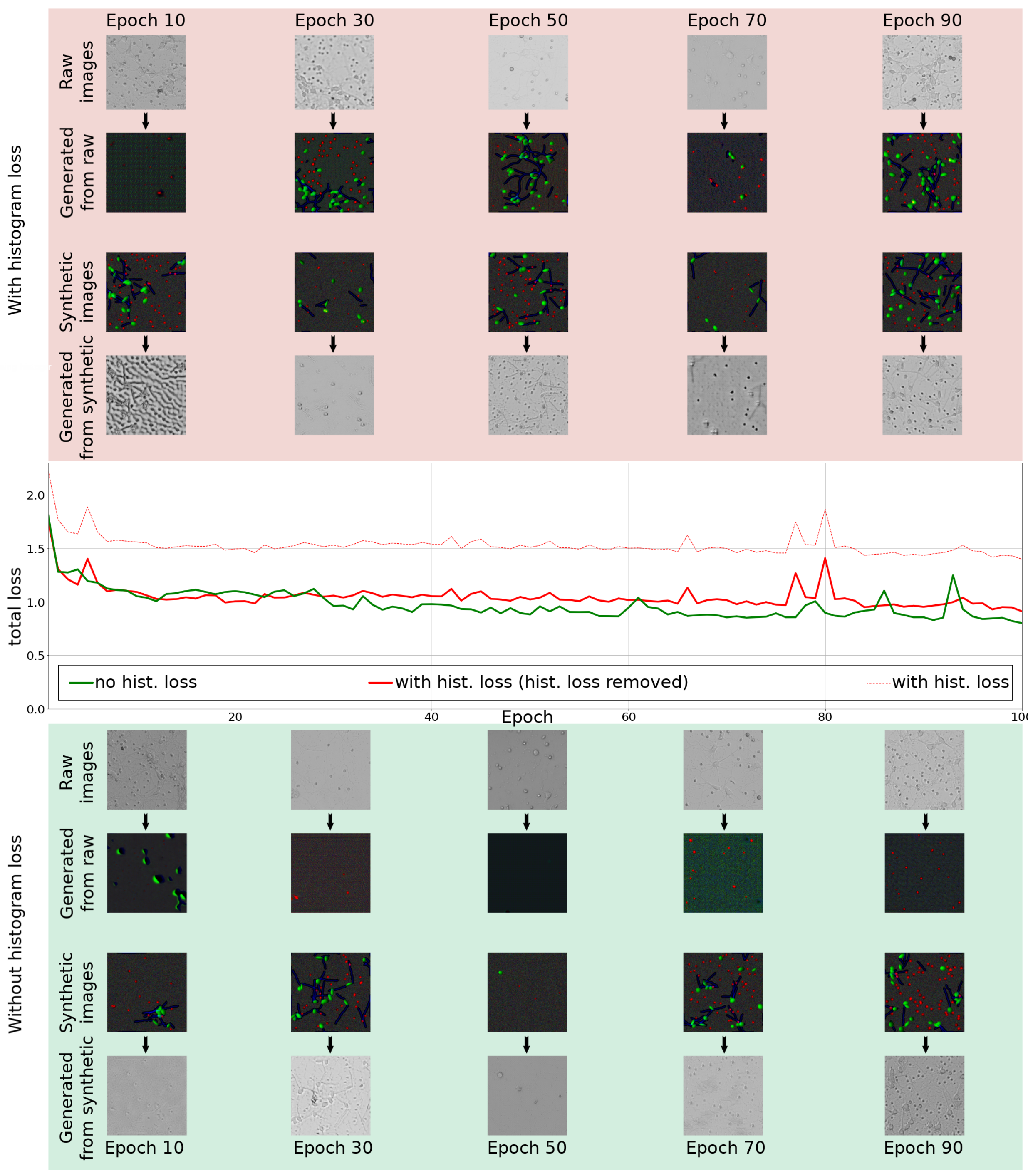

Figure S7: Comparison between having a histogram discriminator versus not having it. The total loss, as defined in Equation S1, is plotted for the first 100 epoch of training in the case where the histogram discriminator is not used (continuous green) and when it is (dashed red line). For better comparison of the two cases, the latter has also been plotted after removing the contributing terms of the histogram discriminator from the total loss (continuous red). Above and below the losses, example generated images are shown for different times during the training when not using a histogram discriminator and when using it, respectively. The authors believe that there are two reasons for the lower total loss when not using a histogram even though the quality of the created images is qualitatively worse. First, the total loss with histogram discriminator is minimized by the network (dashed red) instead of the total loss not considering the histogram losses (continuous red). Second, the lower quality of the generated images helps the discriminators to make better predictions. The corresponding improvement for the loss is bigger than the cost associated with a worse cycle reconstruction.

Supplementary Tables

	Expert 1	Expert 2	Expert 3
Average dead count	33.41	34.39	35.86
Average alive count	11.68	11.26	11.76
Average total count	45.10	45.65	47.62

Table S1: **Average number of neurons per image**: The average number of dead, alive, and total neurons as counted by three different experts. While the average alive count is quite consistent for each expert, the average number of dead cells counted can be off by as much as 7%.

Mean absolute error

	Dead count			**Alive count**		
	Expert 1	Expert 2	Expert 3	Expert 1	Expert 2	Expert 3
Average count	33.4	34.4	35.9	11.7	11.3	11.8
Std in count	19.5	19.9	21.2	8.4	8.1	8.3
Expert 1	-	1.9 ± 2.1	2.7 ± 2.9	-	1.4 ± 1.9	1.2 ± 1.5
Expert 2	1.9 ± 2.1	-	2.2 ± 2.4	1.4 ± 1.9	-	1.1 ± 1.5
Expert 3	2.7 ± 2.9	2.2 ± 2.4	-	1.2 ± 1.5	1.1 ± 1.5	-
Predicting avg	18.1 ± 7.4	18.6 ± 7.1	20.1 ± 6.8	7.2 ± 7.4	6.8 ± 7.1	7.1 ± 6.8
Our approach	6.0 ± 6.2	6.6 ± 6.9	7.9 ± 7.6	**4.3** ± 6.2	4.5 ± 3.9	**4.4** ± 3.7
Count-ception	**5.1** ± 6.4	**5.6** ± 5.7	**4.7** ± 5.3	4.4 ± 4.5	**3.4** ± 3.1	5.8 ± 4.7

Table S2: **Average number of neurons per image**: The average number of dead, alive, and total neurons as counted by three different experts. While the average alive count is quite consistent for each expert, the average number of dead cells counted can be off by as much as 7%.

Post-processing

VGG Dataset

Counting by area: the raw-to-synthetic generated images are the color-labeled versions of the raw images. The images are in a shape of [276,276,3] floats between 0 and 1, where the last 3 channels are the colors. Because the last (blue) channel contains the noise, to convert the colors into numbers, we apply the following transformation to image Im

$$Im[:,:,0] < 0.2 \quad \& \quad Im[:,:,1] > 0.2] \rightarrow 1 \tag{S13}$$

$$Im[:,:,0] > 0.2 \quad \& \quad Im[:,:,1] < 0.2] \rightarrow 2 \tag{S14}$$

$$Im[:,:,0] > 0.2 \quad \& \quad Im[:,:,1] > 0.2] \rightarrow 3 \tag{S15}$$

signifying that we map green regions to 1 (no overlap), red regions to 2 (two cells overlap) and the white regions to 3 (more than 2 overlaps). The other pixels are mapped onto 0. The resulting image, Im_t, is now a [276,276] array of integers between 0 (background) and 3. The resulting transformed image is then summed up and divided by the average cell radius r (5.45 pixels) in the synthetic data. Therefore,

$$\text{Count} = \sum_{i,j=1}^{276} \frac{Im_t[i,j]}{\pi r^2} \tag{S16}$$

Counting by position

The raw-to-synthetic generated images contain the cell shapes in the red channel, and Gaussian maps $G(x, y, x_0, y_0) = e^{-(x-x_0)^2-(y-y_0)^2}$ with a standard deviation of 1 pixel in the blue channel at the center of each cell. We need to find the coordinates x_0, y_0 of each Gaussian map, without knowing how many there are. To that end, the following algorithm is performed:

1. Threshold the image in the blue channel
2. Find all pixel clusters above the threshold
3. For each cluster, perform a fixed-covariance (variance of 1) Gaussian mixture model with a variable number of Gaussians. Choose the number that minimizes the distance between the pixel values and the fit
4. Store all the found Gaussian centers

Correction factor: for each pixel cluster whose maximal pixel value was above 1, but we could not separate into two distinct Gaussians (they are too close), we added a count of 1 to the number of found centers.

Primary cortical neurons

Counting dead neurons: For predicting the location of dead neurons, the red channel of the cycleGAN generated images were Gaussian-smoothed with a mean of half a pixel. A dead neuron was predicted at every peak in the smoothed image that was at least as high as 0.5 (pixels can have values between 0 and 1) and did not have any higher peaks in a distance of 2 pixels.

Counting live neurons: The live neurons were predicted by first creating a binary map B, which was 1 for each pixel of image I, where the sum of the three color channels of the generated images of the second neuron cycleGAN exceeded 0.75. All other pixels were set to 0.

$$B[x,y] = \begin{cases} 1 & \text{if } I_{\text{red}}[x,y] + I_{\text{green}}[x,y] + I_{\text{blue}}[x,y] > 0.75 \\ 0 & \text{otherwise} \end{cases} \tag{S17}$$

From B, all connected pixel clusters were extracted. Islands were discarded, if they contained less than 10 pixels (noise). All remaining islands correspond to one or more live neuron.

For each island, we seek to find the number of distinct colors, since this number corresponds to the number of cells for the given island. Below calculations are done for each island separately. To simplify readability, the below equations do not contain an index for each island. To find the number of live neurons, we first normalized the color vector of each pixel belonging to the island under observation to one.

$$\text{Col}_i = \frac{1}{\sqrt{I^2_{\text{red}}[x_i,y_i] + I^2_{\text{green}}[x_i,y_i] + I^2_{\text{blue}}[x_i,y_i]}} \begin{bmatrix} I_{\text{red}}[x_i,y_i] \\ I_{\text{green}}[x_i,y_i] \\ I_{\text{blue}}[x_i,y_i] \end{bmatrix} \tag{S18}$$

Here, x_i and y_i describe the location of the ith pixel of the island under consideration. In the normalized vectors Col_i, both the green and blue channel encode the same property (see Equation S7). Therefore, the color vector only contains two independent properties, which encode the relative location in the x direction and the relative location in the y direction of the neuron with respect to other neurons. In the next step, these two properties were extracted:

$$W_i = \begin{bmatrix} \text{Col}_i^{(1)} \\ \frac{1-\text{Col}_i^{(2)}+\text{Col}_i^{(3)}}{2} \end{bmatrix} \tag{S19}$$

We call the 2D space in which the vectors W_i lay the color space. After placing each W_i in the colorspace, we determined for each element the distance D_i to the 5th closest W_j. This distance describes how frequent the color of the pixel is.

$$D_i = \text{sort}\left(\{\sqrt{(x_i-x_j)^2+(y_i-y_j)^2 — \forall(x_j,y_i) \text{ in island}}\}\right)_5 \tag{S20}$$

In Fig. S8 we give a graphical explanation of what the above mentioned distance is defined.

Based on all D_i, we chose a threshold δ such, that one third of them where smaller than δ and two thirds bigger than δ. We discarded all elements W_i of an island for which $D_i > \delta$. By doing so, we could only keep W_i

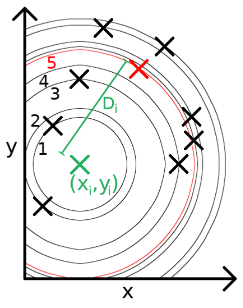

Figure S8: **Distance metric of point in colorspace:** The distance D_i for the i^{th} point (green) in the colorspace is defined as the euclidean distance to the 5^{th} closest other point (red).

that are similar in the colorspace. While this pre-segmentation of the colorspace is not necessary, it simplifies the subsequent clustering.

Of the remaining color vectors W_i, the largest number n was found, for which all n mean locations of an n component Gaussian mixture model (gmm) had an euclidean distance of at least 0.25. It was assumed that an island never had more than 5 neurons ($n \leq 5$). The final number of neurons per island was set to n. The location of these neurons was chosen as the mean of the pixel location belonging to each of the gmm Gaussians.

Benchmarking

We investigated the influence that different object densities, shapes, sizes, and background noise level have on the performance of the approach. For all tests the dead versus live neuronal dataset was used. For each test, the synthetic datasets and training methodology were identical except for the parameter under consideration. The choice of the neuronal dataset for benchmarking is justified by the fact that the shape and size and object numbers here are well defined. We did not change the post processing algorithm. This is not an issue in the case of neuronal density. However, due to the simplicity of post processing, properties like size and background noise can affect for example the peak detection used for dead neurons.

Background noise: The background noise in the synthetic neuronal images used in this work is Gaussian noise with a standard deviation of 0.07. In order to avoid negative pixel values, the mean was set to 0.15 and the pixel values were clipped to lie between 0 and 1. We tested the effect of the background noise by varying the noise standard deviation between 0.007 and 0.35. The mean was adapted appropriately. In video S1, the generated segmentations are plotted over the 200 epochs of training for 4 example images. One can see, that the synthetic data generators have issues if the noise level exceeds a value of 0.07. In general, it takes qualitatively longer for the generators to find a mapping the smaller the noise is. If there is no noise, we could not get the generator to find a mapping (data not shown).

The effect of the noise levels on the mean absolute count error per image is shown in Fig.S9. For noise levels below 0.07, no clear trend is present. While above 0.07 there is some increase in the error, this increase is likely introduced during the post-processing step. Since we count the dead neurons by detecting every peak in the image that is above the value of 0.3, we inevitably will detect noise as neurons as well with a non negligible probability for a Gaussian noise with standard deviation of 0.15 and above. Therefore, we did not plot these prediction errors.

Neuronal density: In order to investigate the effect of the object density distribution on the quality of the segmentation, we varied the mean number of neurons in the synthetic dataset between half and twice as much as in the raw data. More precisely, the actual point mass functions of the dead and live image is known since we know a priori what the viability of the neurons is and how many neurons there are per image in total. The precise distributions are described in the results of the main text. Since the neurons have been seeded

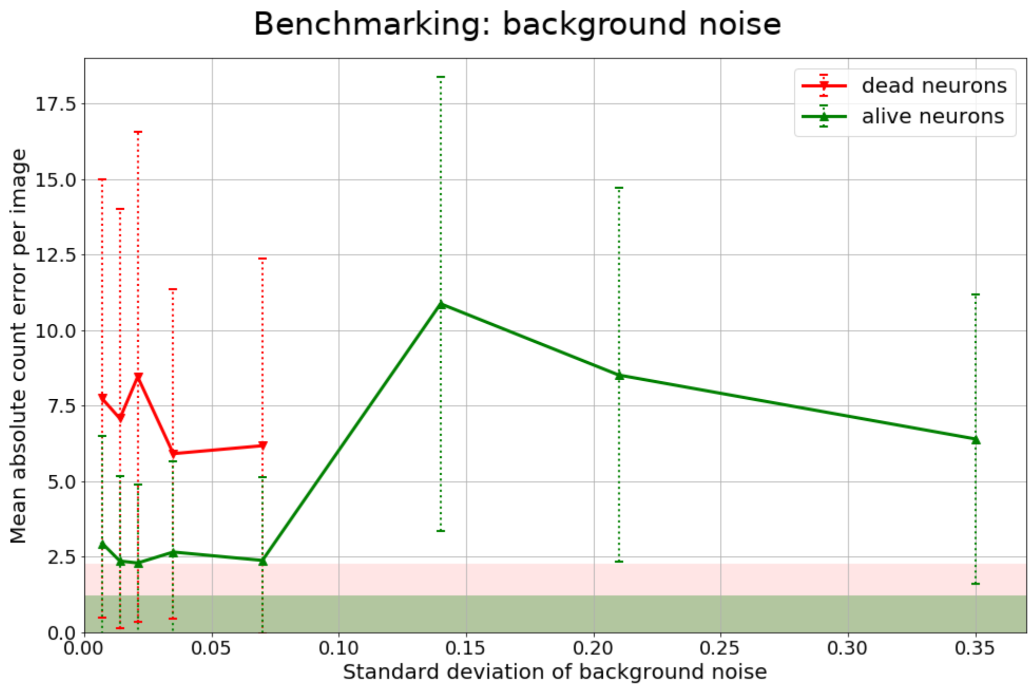

Figure S9: **Effect of background noise on segmentation:** The mean absolute count error is plotted for each image for the dead and live neurons with respect to the background standard deviation (Gaussian noise) in red and green, respectively. The red and green overlaid regions describe the average level of average disagreement between the three experts.

at two different densities, the distribution is a sum of two Poisson distributions. The distributions are plotted in white in Fig.S10 for the raw images. We investigated the effect on the mean absolute error of scaling the expected value of the two Poisson distributions by a factor of α in the synthetic dataset with respect to the raw distributions. The distributions investigated are also plotted in Fig.S10.

Video S2 shows the generated images for the different densities during training. While all investigated cases find a meaningful mapping between raw and synthetic data, the network trained on images with high synthetic densities qualitatively overestimate the number of neurons, while the networks trained with low synthetic densities underestimate the number of neurons. This is not surprising, since we assume the prior neuron distribution to have an effect on the posterior neuron distribution in the segmentation. Quantitatively, the effect can be seen in Fig.S11, where the mean absolute count error is plotted with respect to α. The error is almost flat for α values between 0.9 and 1.3. It seems that the actual object distribution must not be known precisely but can be off by about 20 to 30%. Furthermore, better results could be achieved than shown in Table 2 and S2 when overestimating the actual distribution by 10%.

Object shape: We investigated the effect of the shape of the neurons in the synthetic dataset on the mean absolute error. We described the shape of the objects by a superellipse:

$$\left|\frac{x}{a}\right|^n + \left|\frac{y}{b}\right|^n \leq 1, \tag{S21}$$

where a and b are the semi-major and semi-minor axis of the superellipse and n defines the shape. For example, for $n = 1$ the superellipse is a parallelogram, for $n = 2$ it is an ellipse and for $n = \infty$ a rectangle. We scaled a and b in order to guarantee that the area of the superellipses does not depend on n. In the next paragraph we will investigate the effect of different object sizes.

Video S3 shows how the generated images compare during training for different values of n. The absolute mean error of the neuron counts are given in Fig.S13. One can see that UDCT first creates elliptical patterns independent of the value of n, before mapping the respective shapes. We suspect this is due to the fact that

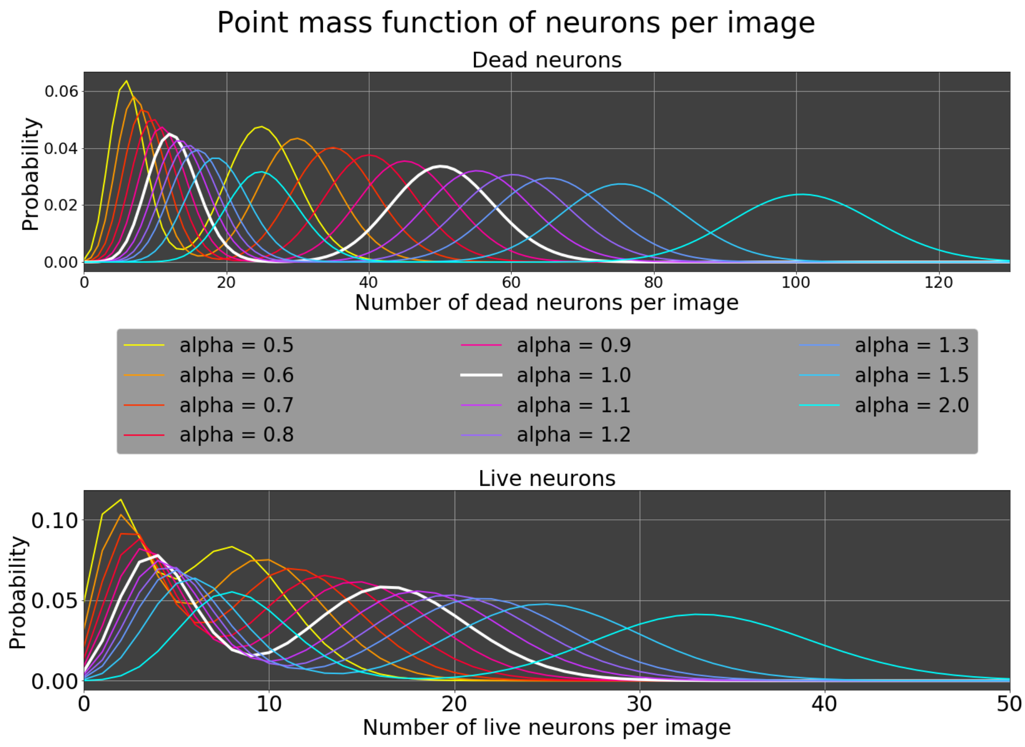

Figure S10: **Neuron densities used for benchmarking:** The point mass functions for the dead (top) and live(bottom) neurons is plotted for different parameters of α. The parameter α describes by how much the expected value of the sum of the two Poisson distributions has been scaled in the synthetic data with respect to the actual distribution. The latter is plotted in white.

ellipsoids are easier to create with neuronal networks than star-like shapes and because neurons have similar shapes. The relationship between shape and count loss is not obvious. The high fluctuations in the plot are likely due to the post processing.

Object size: We observed the effect of changing the size distribution of objects in the synthetic dataset with respect to the object sizes in the genuine data. We scaled the area of an object by a factor of 0.5 two 2. Video S4 shows the generated images during the training period for different size objects. The effect of the size on the mean absolute error count is shown in Fig.S12. The closer the object sizes match, the better the loss is in general. However, if the distributions are off by less than 20%, this effect appears to be negligible.

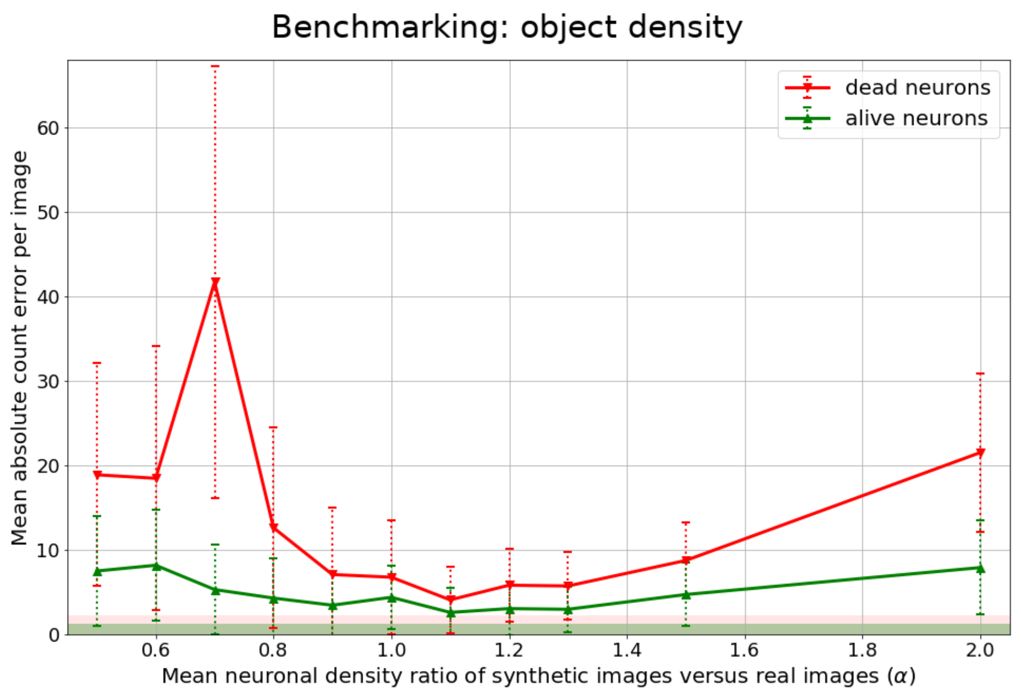

Figure S11: **Effect of object density on mean absolute error:** The mean absolute count error is plotted for each image for the dead and live neurons with respect of the parameter α, which describes by how much the expected value of the sum of the two Poisson distributions has been scaled in the synthetic data with respect to the actual distribution. The point mass functions of the different distributions are given in Fig.S10.

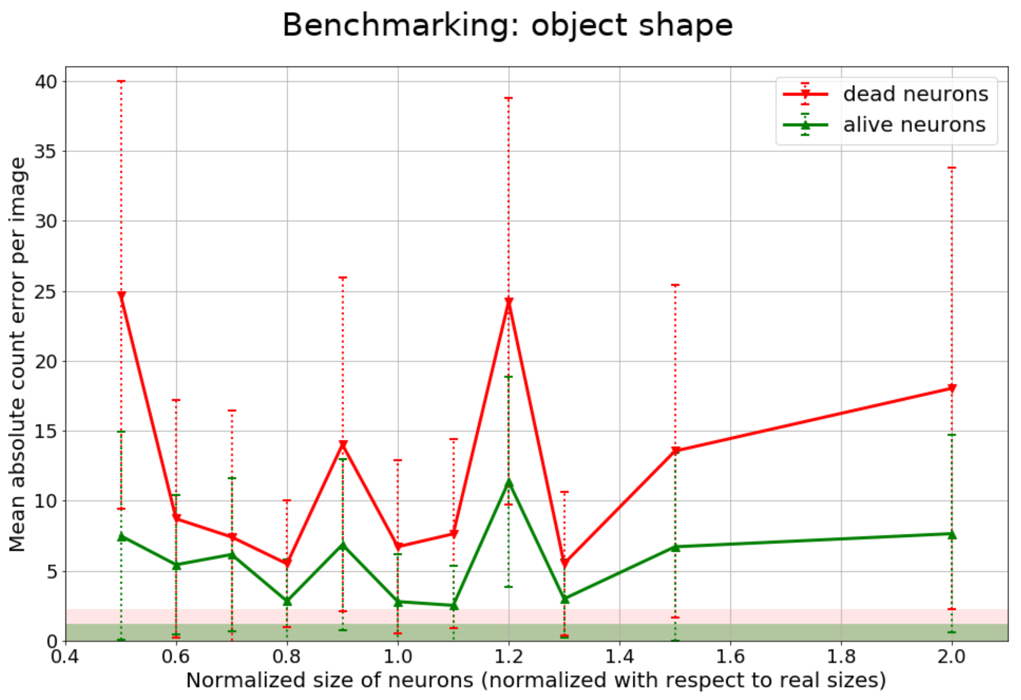

Figure S12: **Effect of object size on mean absolute error:** The mean absolute count error is plotted for each image for the dead and live neurons with respect of the normalized mean size of the synthetic neurons.

References

[1] Zhu, J.-Y., Park, T., Isola, P. & Efros, A. A. Unpaired image-to-image translation using cycle-consistent adversarial networks. *arXiv preprint* (2017).

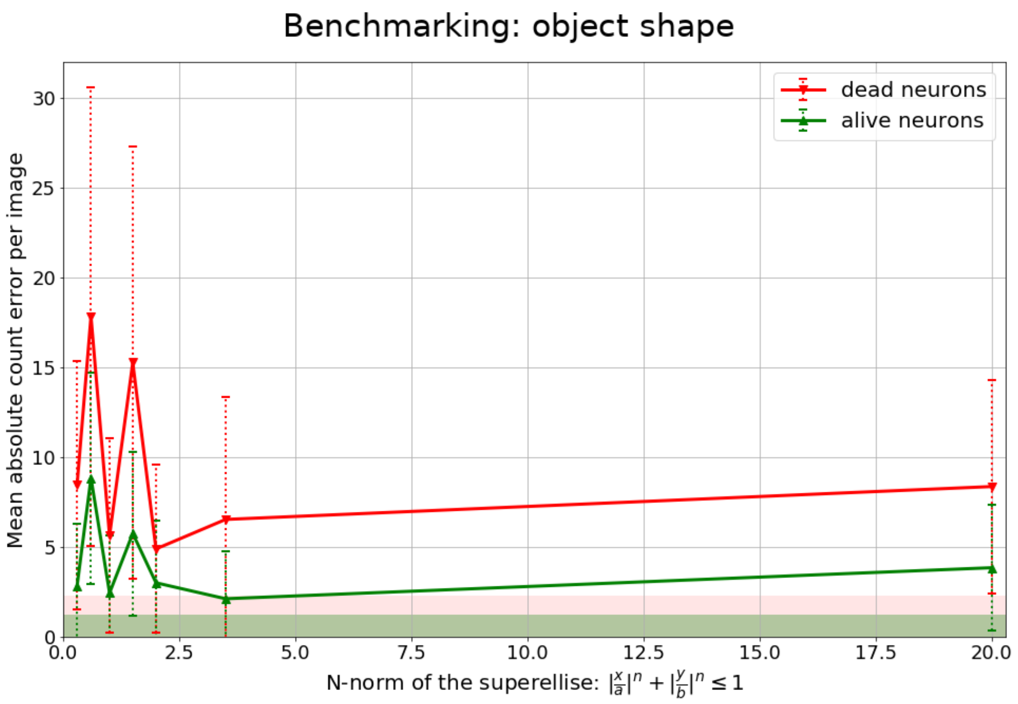

Figure S13: **Effect of object shape on mean absolute error:** The mean absolute count error is plotted for each image for the dead and live neurons with respect of the parameter n, which is modulating the shape of the synthetic neurons. The exact relationship is described in equation S21.

[2] Shrivastava, A. *et al.* Learning from simulated and unsupervised images through adversarial training (2017). URL `http://arxiv.org/abs/1612.07828v2; http://arxiv.org/pdf/1612.07828v2`. `1612.07828v2`.